Journal of Applied Ecology 1997, **34**, 418–432

Analysis of desert plant community growth patterns with high temporal resolution satellite spectra

ALBERT J. PETERS*, MARLEN D. EVE*, E. HOWARD HOLT† and WALTER G. WHITFORD‡

**Centre for Advanced Land Management Information Technologies, Conservation and Survey Division, Institute of Agriculture and Natural Resources, University of Nebraska-Lincoln, Lincoln, Nebraska 68588–0517, USA; †Department of Geography, New Mexico State University, Las Cruces, New Mexico 88003, USA; ‡US Environmental Protection Agency, Environmental Monitoring Systems Laboratory, Las Vegas, Nevada 89193, USA*

Summary

1. The study of a desert landscape consisting of C_3 shrublands and C_4 grasslands demonstrated the feasibility of mapping desertification processes on a regional scale using time-series satellite images, and demonstrated the potential for monitoring desertification processes through time.

2. Fifteen meteorological satellite images of southern New Mexico, spread over the growing season of 1989, were processed to yield images of normalized difference vegetation indices. Computer classification of these images and comparison with extensive ground measurements confirmed the identification of the major classes of shrubland, grassland and mixed shrub and grass areas.

3. Our high-resolution temporal approach is shown to permit the accurate identification of vegetation types even under conditions of sparse vegetation cover. The phenologies of grassland and shrubland were revealed in the time series of satellite images. We used this feature of the data to overcome the tendency of the strong radiation signal from bare soil to mask the biomass signal.

4. Comprehensive comparisons with ground measurements confirmed the accuracy of the biomass identification for local areas within the Jornada Experimental Range, and justified extrapolation of the classification to a larger adjacent area.

Key-words: Chihuahuan Desert, phenology, satellite imagery, vegetation index.

Journal of Applied Ecology (1997) **34**, 418–432

Introduction

The primary focus of our research is the use of a sequence of single-date AVHRR (Advanced Very High Resolution Radiometer) images to derive information on growth characteristics and phenology of vegetation in a semi-arid area of southern New Mexico. The measure used for estimating vegetation photosynthetic activity is the normalized difference vegetation index (NDVI), (NIR − VIS)/(NIR + VIS), where NIR is the reflectance radiated in the near infrared waveband and VIS is the reflectance radiated in the visible red waveband of the radiometer.

We studied an area where the amount of cover in native plant communities, consisting of desert grassland and desert shrub, is often less than 40% (Peters *et al.* 1993). At such low percentages of biomass cover previous investigators have had difficulty interpreting satellite-derived vegetation indices (Elvidge & Lyon 1985; Frank 1985; Huete & Jackson 1987). Our approach provides a technique to overcome this difficulty. Our methodology is based on a vegetation 'signal' derived from mapping polygons that are carefully co-registered throughout the time series of imagery, thus normalizing the soil background response. This vegetation signal would not be discernible in a single date of imagery, but does provide meaningful information when a carefully controlled time series of imagery is prepared for an entire growing season, and the area of measurement remains constant for each sample (Peters & Eve 1995). This approach increases our ability to estimate vegetation cover, composition and physiological status into landscape models at the regional scale, and could enhance our understanding of status and trends in biodiversity by identifying changes in the shape, size and condition of habitats (US Environmental Protection Agency 1994). Our methods offer the potential of a simple

'real-time' indicator of landscape dynamics through the mechanism of satellite-derived pixel changes on a temporal scale. Detected changes could represent landscape modification or degradation through time periods of significance to land managers.

The AVHRR is commonly accepted as preferred over the LANDSAT and SPOT radiometers for temporal studies of vegetation because the latter instruments image a given area too infrequently, especially when cloud cover problems are taken into account. Even with the daily pass of AVHRR over the study area, steps are normally taken to mitigate the effect of cloud cover. This is routinely accomplished by using a week's data (or more) to produce a composite image consisting of the brightest NDVI values of each pixel of the geographically registered set of images (Holben 1986). It is assumed that this value represents a cloud-free signal. In this way Goward, Tucker & Dye (1985), Justice *et al.* (1985) and Tucker, Townshend & Goff (1985) have used AVHRR data at a global resolution scale of 4 km to study the vegetation patterns of North America, the entire globe and Africa, respectively. Tucker & Choudhury (1987) produced cloud-free NDVI single date images by using AVHRR thermal radiation as a cloud mask. The resulting images were used to study drought conditions in the Sahel. Millington *et al.* (1994a) have conducted a comprehensive study of land cover for the entire continent of Africa south of the Sahara, emphasizing the presence of woody biomass. They used global vegetation index data (AVHRR-NDVI) at 8-km resolution.

AVHRR data have been used to study vegetation conditions in 17 western states of the USA in 1989 (Eidenshink & Haas 1992). Daily data were combined into biweekly data sets throughout the growing season. The results led to the conclusion that temporal NDVI derived from AVHRR data is a useful tool for monitoring the dynamics of natural resource areas on a regional basis. Tucker & Choudhury (1987) have also used composite AVHRR data. They studied drought in northern Africa in the period 1984–86 and showed that the composite data revealed the effects of drought by detecting reductions in photosynthetic activity during the growing season.

Millington *et al.* (1994b) have used a core zone approach to identify land cover classes in Pakistan in a study of AVHRR-NDVI and moisture availability relationships. Millington & Pye (1994) have emphasized the importance of combining ground-based and satellite observations in the study of dry land sites.

We have been successful in retaining the accuracy of single-date images by restricting our study to a more local area which, more often than not, produced cloud-free images. In the minority of cases where clouds were present we followed Tucker & Choudhury (1987) in using data from the thermal channel to provide a cloud mask which was then used to screen the NDVI image.

Lambin & Strahler (1994) have also taken the approach of using a temporal sequence of AVHRR images and analysing the differences between them. This is described as change vector analysis. They show that this approach captures the maximum detail contained in the time trajectory of the indicator NDVI. They applied the technique to the Sahel of west Africa in the period 1987–89, and they used image compositing to remove most cloud formations. In contrast, other researchers have used Landsat MSS data to develop models and describe conditions on the rangelands of arid Australia (Pickup & Chewings 1994; Pickup 1994; Pickup 1995), and found that because of the relatively large pixel size (1·1 km), AVHRR data are not suitable for grazing impact studies (Bastin, Pickup & Pearce 1995).

Turner (1989) shows that spatial patterns of biomass affect many ecological processes and that the long-term maintenance of biodiversity requires the preservation of appropriate spatial patterns of biomass and habitat. Therefore such studies of vegetation patterns as we report here make a contribution to these issues of environmental concern.

In our study, we did not attempt to quantify any vegetation properties on the basis of the satellite-derived vegetation indices, but rather analysed relative differences in the composition of dominant groups of species from phenological patterns, discernable from satellite coverage. The study of these differences in dominant species is a useful tool in monitoring arid ecosystems. Because our emphasis is on the behaviour of dominant species, rainfall and soil spatial variability were not considered in our analysis. Computation of a normalized vegetation index and the implementation of standardized analysis polygons throughout the time-series data adequately accounted for soil colour differences found throughout the study area.

The potential for separating the dominant vegetation using AVHRR data rests on an unsupervised image classification strategy that is based on time-series differences in the phenology of native plant species. This method is similar to the usual use of unsupervised image classification strategies which use clustering within feature space on multiple wavebands. In southern New Mexico, the dominant native shrubs are *Prosopis glandulosa* Torr. (mesquite), *Larrea tridentata* (DC.) Cov. (creosotebush) and *Flourensia cernua* (DC.) Comp. (tarbush). *Prosopis glandulosa* is a winter deciduous shrub that initiates leaf and stem growth between late April and late May depending upon landscape position. Most leaf production in *P. glandulosa* in the Chihuahuan desert occurs at nodes that are more than 1 year old (W. G. Whitford, unpublished data). In a study of the phenology of *P. glandulosa*, Nilsen *et al.* (1987) found two leaf cohorts per year, with the second only a fraction of the first. Most leaf production (80–90%) occurred on nodes older than 1 year and in general the seasonal progress of growth was unrelated to seasonal fluctuations in pre-

cipitation and temperature. *Larrea tridentata* is an evergreen shrub that attains maximum growth in the cool months of April–May and October–November (Fisher *et al.* 1988). Both *P. glandulosa* and *L. tridentata* produce new leaves during the spring; the amount of winter–spring rainfall influences the amount of foliage produced but not the timing (Fisher *et al.* 1988; W. G. Whitford, unpublished data). The timing of spring leaf production in *F. cernua*, a winter deciduous C_3 shrub, is dependent upon the distribution and amount of winter–spring precipitation. The dominant perennial grasses of the Chihuahuan Desert are C_4 species that require relatively high nighttime temperatures to produce new growth. The timing of green-up and maximum growth of these grasses is primarily a function of water availability (Stephens & Whitford 1993). Grasses are primarily *Hilaria mutica* (Buckl.) Benth. (tobosa grass), several species of *Bouteloua* spp. (grama), *Aristida* spp. (three-awns), *Sporobolus* spp. (dropseeds), *Scleropogon brevifolius* Phil. (Gram.) (burrograss) and several species of *Muglenbergia* spp. (muhly). Differences in phenological patterns of the most abundant C_3 shrubs and the C_4 grasses provide an opportunity to identify and separate pixels representing areas with high grass cover from pixels representing areas with one or other of the C_3 shrubs using time-series based unsupervised image classification techniques. The differences across the landscape are likely to be greatest in a year when winter and spring rainfall is insufficient to support spring growth of annual plants. This means that a modest spring green-up attributable mainly to C_3 shrubs is expected, whereas after the monsoon late summer rains the green-up will be mainly due to C_4 grasses. We therefore chose satellite imagery for a year characterized by a dry winter and spring, 1989, to optimize the likelihood of validating our approach to semi-arid biomass characterization using satellite multitemporal imagery. The general validity of our approach awaits a further study using multi-year data.

Materials and methods

STUDY AREA

The study area included a portion of the northern Chihuahuan Desert of southern New Mexico, USA (Fig. 1). This region lies within the Basin and Range physiographic province of the south-western USA and is characterized by very rugged, often conifer-clad, mountains surrounded by gently sloping intermountain basins. It extends from the Black Range in the west to the Sacramento Mountains in the east, and is bisected by the Sierra Oscura-San Andres Mountains and the Rio Grande. Two additional mountain ranges, the San Mateo and Magdalenas, are located in the north-western corner. Elevations are approximately 1250 m asl in the relatively flat to gently rolling non-mountainous areas.

The climate is typical of a desert region with annual rainfall of 230 mm or less. Monsoonal moisture, often associated with violent summer thunderstorms during the mid-July–mid-September period, provides most of the annual rainfall. Annual average temperatures are approximately 24·7 °C, and the warmest daily high temperatures occur in June (34·4 °C). Potential evaporation can be as much as 10 times the annual precipitation in the area (Paulsen & Ares 1962).

We focused the project on a field calibration area within the south-western portion of the Jornada Experimental Range (JER), which was historically a grassland basin (Buffington & Herbal 1965) (Fig. 1). The JER has been operated as a rangeland research facility of the US Department of Agriculture since 1912. We chose the JER because of its: (i) network of rain gauges; (ii) records of management for large pastures; (ii) historical database of vegetation, soils and land-use patterns; and (iv) recent survey data on composition and cover of vegetation. An additional field extrapolation area was established to the west of the JER to test the capability to extrapolate our information to a regional scale (Fig. 1).

COVER AND COMPOSITION OF THE FIELD CALIBRATION AREA

Cover and composition for each vegetation class were obtained by the line intercept method (Canfield 1941; Buell & Cantlon 1950). Four 90-m lines were read in each land area. The first line was chosen at random by an odometer reading from a road adjacent to or traversing the mapped vegetation class. A random compass heading was chosen and the origin of the first line was established by pacing between 100 and 200 m from the road location. Subsequent lines were located by a random compass heading and random number of paces between 100 and 200 m. The canopy intercepted by the line was recorded to the nearest cm. It was found that each of the classes that were measured on the Jornada represented a unique composition of plant species. Our field measurements were not intended to demonstrate statistical significance, but only to verify the mix of vegetation within each class and for qualitative comparison with the satellite NDVI measurements.

AVHRR DATA CHARACTERISTICS

Operational weather satellites carry optical sensors that provide the ability to monitor fluctuations and changes in land surface conditions systematically over areas of regional and global scale (NOAA 1991; Tucker, Dregne & Newcomb 1991; Eidenshink & Hass 1992).

Data from the NOAA-10 satellite using multispectral high-resolution picture transmission (HRPT) were obtained for the 1989 growing season. Data from the HRPT mode are transmitted con-

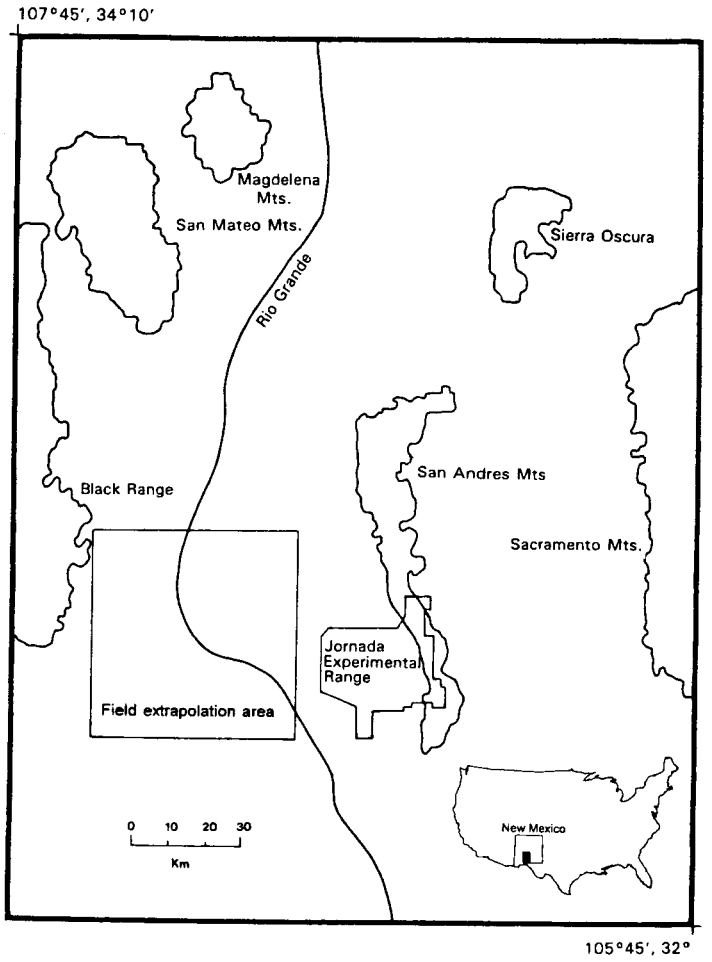

Fig. 1. Location and detail of the study area within the state of New Mexico, USA.

tinuously in real time, and have a spatial resolution of 1100 by 1100 metres at satellite nadir. Additional characteristics of the AVHRR include its daily coverage, relatively low cost of $100 US per scene, high radiometric resolution (1024 gray-levels) and synoptic view (2400 km). The morning overpass of NOAA-10 occurs at 07·30 on the equator and at 07·20 local time in our study area (NOAA 1991). We requested data from the early morning overpass at 15 dates during the growing season. Usually, morning-acquired data minimize cloud contamination and atmospheric dust compared with afternoon data, when thermal heating increases wind and accompanying dust and also cloud cover. We were aware of the likelihood of strong anisotropic reflectance effects due to low sun angles in the early morning satellite overpass. We minimized these effects by utilizing only near-nadir imagery and by keeping our ground study area in the backscatter portion of the image. Additionally, our processing algorithm adjusted for changes in solar angle across each scan line.

We purchased 15 dates of raw HRPT data from the EROS data centre in Sioux Falls, South Dakota. Our criteria for image selection were: (i) near nadir acquisition within 7·5 degrees of the study area; (ii) minimum cloud contamination; and (iii) temporal distribution as uniform as possible throughout the growing season. We acquired single-date imagery because we wanted to maintain control over the above variables and ensure near-nadir viewing geometry.

AVHRR IMAGE PREPROCESSING

The original 10-bit radiometric resolution of the data was retained throughout the analysis. A one-step algorithm combining georeferencing and radiometric calibration, and normalization for solar irradiance variation due to sun angle, using calibration parameters provided in the data sets was implemented (Di & Rundquist 1994) (Fig. 2). Each pixel in the raw data represented variable land areas due to the curvature of the earth and the off-nadir scan angles of the satellite sensor. This causes features to appear geometrically distorted on the raw image. An image-processing step adjusts for this distortion by georeferencing the raw data to a latitude and longitude co-ordinate system. Each 1·1 km pixel was calculated to be the equivalent of 0·00992 degrees of latitude (Y) and 0·01177 degrees of longitude (X), based on the coordinates for the location of the study area in southern New Mexico. Nearest-neighbour pixel resampling was utilized in the georeferencing process to maintain the greatest

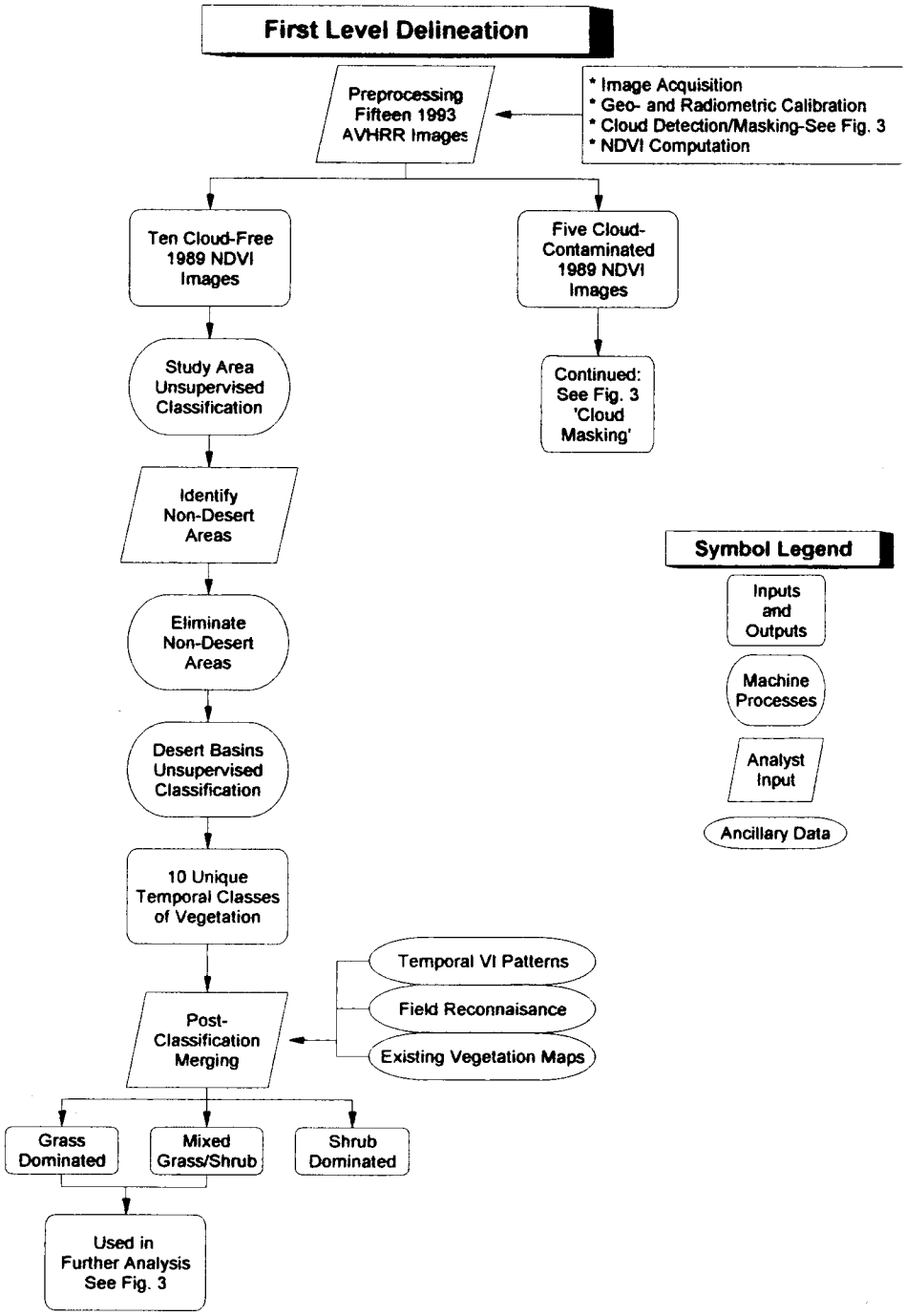

Fig. 2. Steps involved in delineation of general land cover types on satellite data.

possible spatial accuracy (Jensen 1995). Each date of imagery was then precisely co-registered across the study area.

CLOUD MASKING

Clouds were present in five dates of imagery and were eliminated through a masking technique (Tucker & Choudhury 1987) (Fig. 3). We accomplished this with visual analysis of the thermal channel from the AVHRR sensor (10·3–11·7 μm), which responded to clouds by registering much cooler temperatures than that typical of the land surfaces. A binary cloud mask was produced for each date of imagery, with every pixel contaminated by a cloud converted to zero and all other pixels given a value of one. Multiplication of the imagery by the cloud mask converted cloud-obscured pixels to a value of zero, thus eliminating them from the analysis. Atmospheric attenuation corrections were accomplished using histogram minimization techniques which reduced and normalized path radiance (Jensen 1995).

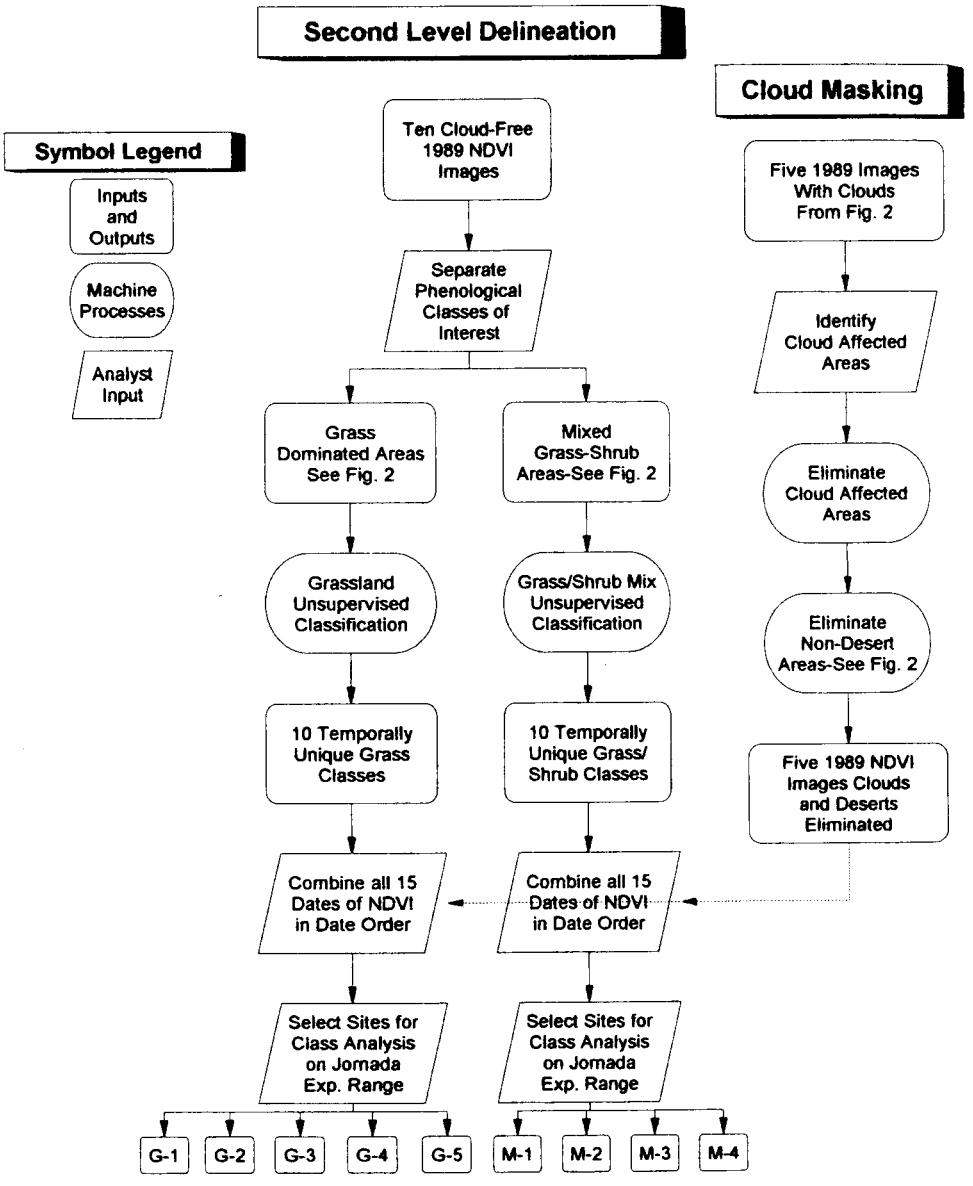

Fig. 3. Steps involved in delineation of specific plant communities used in analysis of satellite data.

VEGETATION INDEX

Typically, successful vegetation discrimination on the basis of a satellite image depends upon the contrast in spectral radiance between vegetation and the surrounding soil background. Maximum contrast is usually observed in the red- and near-infra-red wavelengths. As leaf cover increases, chlorophyll absorbs an increasing fraction of red light. Near-infra-red is strongly reflected due to the structural properties of leaves and resulting high degree of scattering in the plant canopy (Tucker 1979).

A mathematical quantity referred to as the normalized difference vegetation index (NDVI) is routinely calculated from AVHRR data due to its sensitivity to the presence and condition of green vegetation (Huete & Jackson 1987; Lillesand & Kiefer 1994). The formulation for this index is: NDVI = (NIR − RED)/(NIR + RED), where NIR refers to near-infra-red reflected energy (0·725–1·10 nm) and RED refers to red-reflected energy (0·58–0·68 nm). Calculation of the NDVI results in pixels with a theoretical index value between −1·0 and + 1·0. Vegetated areas will generally yield high index values, water will yield negative values, and bare soil will result in values near zero (Lillesand & Kiefer 1994).

UNSUPERVISED TEMPORAL IMAGE CLASSIFICATION USED TO MASK NON-DESERT VEGETATION

An unsupervised classification algorithm was implemented on a temporal image comprising 10 dates of co-registered cloud-free NDVI data. These calculations are based on per pixel differences in the growing season activity of vegetation as detected by the NDVI imagery. As a result, we were able to recog-

nize areas of forested mountain slopes, agricultural land and riparian vegetation, all of which have a NDVI response that is higher than that in the desert basins. An image mask was produced which was then implemented on all 15 images to remove non-desert vegetation that was not of interest in our study (Figs 2 and 3). If retained, these non-desert types of ground cover would dominate the subsequent unsupervised classification process with irrelevant classes of vegetation.

DERIVATION OF PHENOLOGY OF PLANT GROWTH

To isolate further scene variance related to the phenology of plant growth in the desert basins during the growing season, we implemented an unsupervised temporal classification algorithm on the deserts of the entire study area on 10 dates of cloud-free images. This resulted in 10 regions of plant activity reflecting different development stages during the growing season. The temporal signatures of each region were compared and evaluated using the statistical differences between them and a visual analysis of the resulting pixel mapped areas. Field data and existing vegetation maps were also studied and a process of post-classification merging led to the identification of three distinct cover classes for the entire desert area within the study boundaries. These were subsequently identified as the typical phenophases of grass, shrub and grass/shrub mix (Figs 3, 4 and 5).

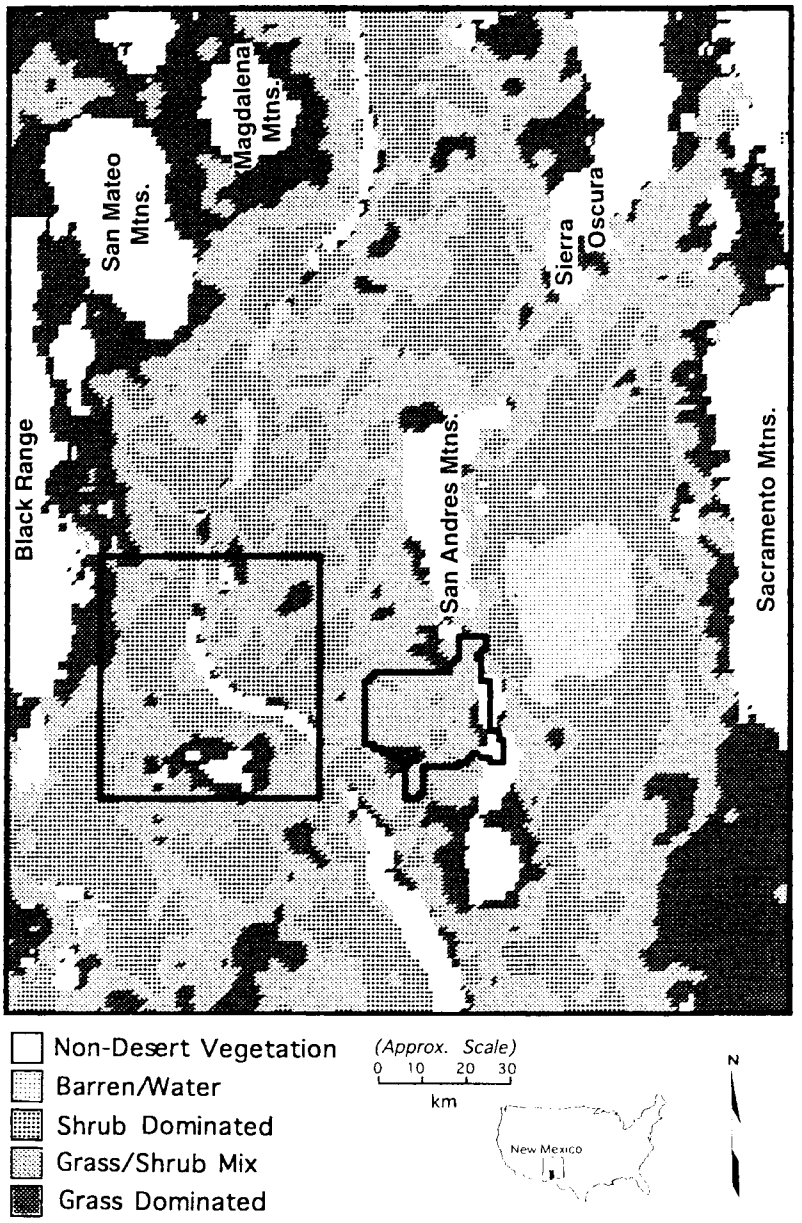

Fig. 4. Location of non-desert vegetation, barren/water, shrub, mixed grass/shrub, and grass-dominated plant communities. The rectangular polygon (lower left) is our field extrapolation area and the irregular polygon in the lower centre is the boundary of the Jornada Experimental Range, which encloses our field extrapolation area in the south-western corner.

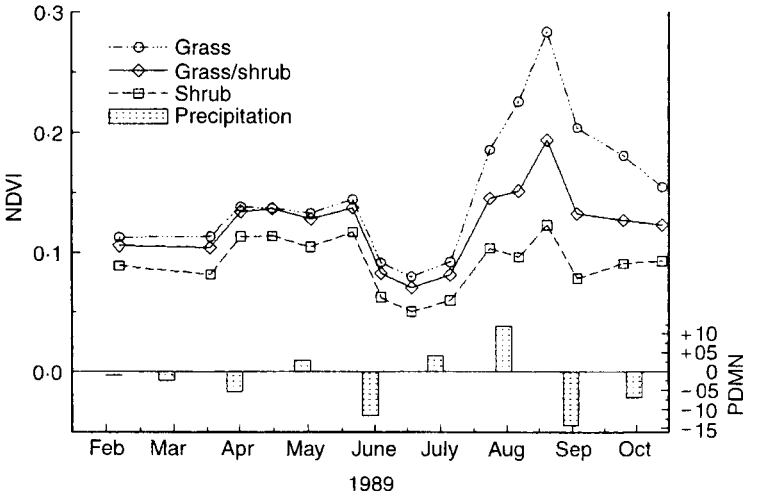

Fig. 5. Satellite derived per-class average temporal normalized difference vegetation index (NDVI) values for grass, mixed grass/shrub, and shrub-dominated vegetation classes. These curves resulted from the post-classification merging of 10 temporal classes in the entire desert of the study area. Precipitation departure from monthly normal (PDMN in mm) was derived from the Southern Desert climatic division of New Mexico (NOAA 1989).

Results

EVALUATION OF THE GENERAL LANDCOVER CLASSIFICATION

In 1989, southern New Mexico experienced below average rainfall from winter through to early summer (Table 1) (NOAA 1989). From the growth-characteristic response graphs of average NDVI values for all pixels in each class (Fig. 5), it could be noted that spring green-up was also extremely limited due to diminished rainfall. Also evident were decreased photosynthetic activity (or senescence) during the hot-dry months of June–July and the green-up resulting from the monsoon rains (July–August). Relatively homogeneous grasslands showed the strongest greenness peak throughout the growing season, primarily due to higher percentage cover, followed by the vegetation class of grass/shrub mix. Shrub-dominated areas had the lowest greenness peak (Fig. 5), and the lowest percentage cover. After careful ground-truth analysis and comparison with existing vegetation maps, we were satisfied that our first-stage temporal classification had resulted in accurate delineation of these major desert plant communities. It also provided us with a vegetation map from which standard areas could be selected throughout the time series and which would be used to normalize our analysis for soil background colour differences through the entire sequence of the image data. We believe that utilization of AVHRR imagery from a year with limited spring and early summer rainfall facilitated the use of greenness peaks to separate grassland from shrub-dominated land areas.

Table 1. Thirty-year average monthly and annual precipitation (1951–80) in comparison with monthly and monthly departure from average for 1989 in the Southern Desert Climatic Division of New Mexico, USA

	1951–80 Average	1989 Actual	Departure
January	61·26	13·21	−3·05
February	12·95	11·94	−1·01
March	11·94	9·65	−2·29
April	5·59	0·25	−5·34
May	6·60	9·40	2·80
June	12·70	1·02	11·68
July	53·85	57·91	4·06
August	53·34	65·28	11·94
September	36·07	21·84	−14·13
October	25·65	18·80	−6·85
November	11·18	1·02	−10·16
December	17·53	12·95	−4·58
Total	263·66	223·27	−40·39

EVALUATION OF GRASS AND MIXED GRASS/SHRUB AREAS

Our remaining analyses were conducted on the grass and mixed grass/shrub vegetation categories. We found that these two categories were present on the Jornada, facilitating our ground verification efforts (Figs 1 and 6).

First, the image data corresponding to the grassland category were extracted from the total image database. Then an unsupervised multi-temporal image classification was performed, resulting in the identification of 10 types of grass-dominated areas within the major category of grassland. Five of these types (G1–G5) were well represented within our field calibration area on the JER and typical sites were identified by personal observation in the field (Fig. 6).

Secondly, the image areas corresponding to the mixed grass/shrub areas were filtered from the data-

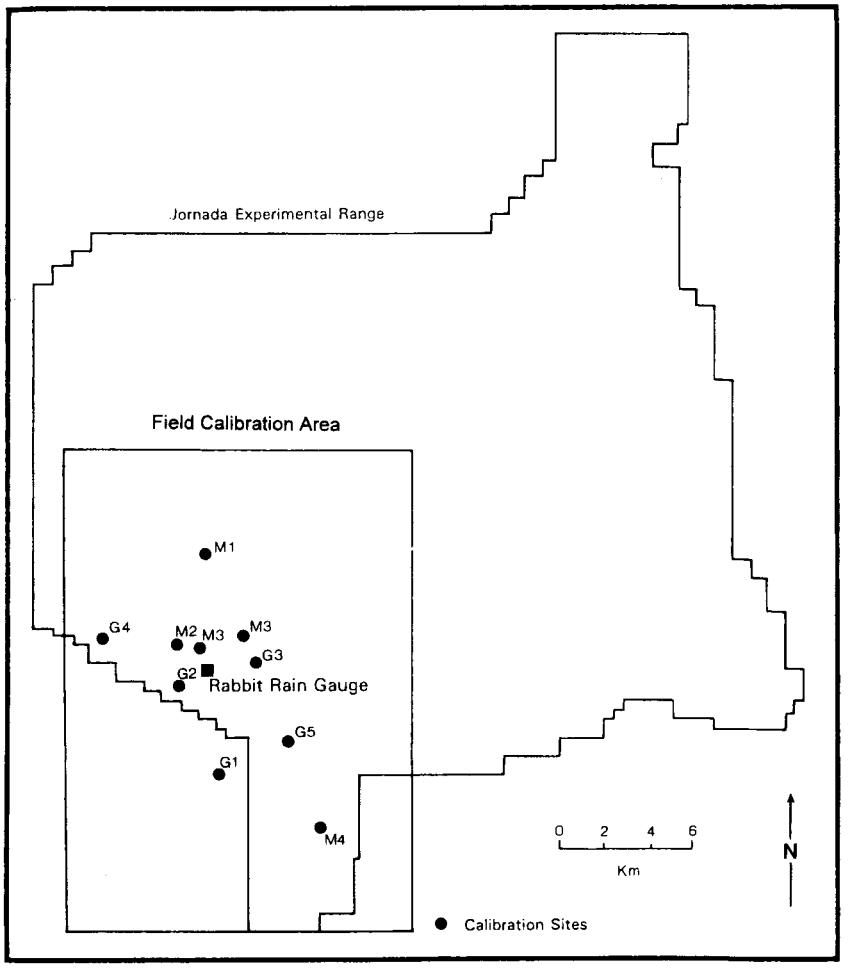

Fig. 6. Location of the field calibration area on the Jornada Experimental Range. Sites used to calibrate mixed grass/shrub communities are identified as M1–M4, and those for the grass-dominated communities as G1–G5.

base and, by a similar procedure, 10 types of the mixed grass/shrub category were distinguished. Then typical sites for the four best represented within our field calibration area on the JER (M1–M4) were identified by personal observation in the field (Fig. 6).

FIELD CALIBRATION AND TESTING

Working maps of classes G1–G5 and M1–M4 (Figs 7 and 8) were overlaid with road and windmill locations for field location and reference. We conducted a field reconnaissance survey to verify qualitatively that classes on the maps corresponded to distinct vegetation conditions at our field calibration area. We located sites for which we had available field data, thus identifying vegetation classes where field data were still needed.

PHENOLOGICAL CHARACTERISTICS OF THE DOMINANT SPECIES

To interpret seasonal NDVI graphs derived from mapped vegetation classes, it is necessary to understand some of the phenological characteristics of the dominant species. *Prosopis glandulosa* is a deep-rooted, winter deciduous, C_3 shrub with a predictable phenology. *Prosopis glandulosa* produces new leaves, flowers and fruits in late April through to mid-June. In years with sufficient winter–spring rainfall, *P. glandulosa* will also produce stem elongation and additional leaf area. *Gutierrezia sarothrae* (Pursh.) Britt. and Rusby (snakeweed), a partially winter deciduous C_3 sub-shrub, produces new foliage in years with adequate winter–spring moisture but in dry years behaves more like a C_4 grass. The other dominant shrub of the northern Chihuahuan Desert, *Flourensia cernua* is a winter deciduous C_3 shrub that exhibits a temporally predictable phenology with morphological flexibility. In years with a dry winter–spring, *F. cernua* produces small scale-like leaves in May–early June. This foliage is insufficient to contribute to a significant NDVI spring peak. With increased moisture availability, *F. cernua* will shed the small leaves and replace them with larger ones. None of the C_4 grasses produces new foliage in years with dry spring seasons. In years with relatively wet springs, *Sprobolus flexuosus*

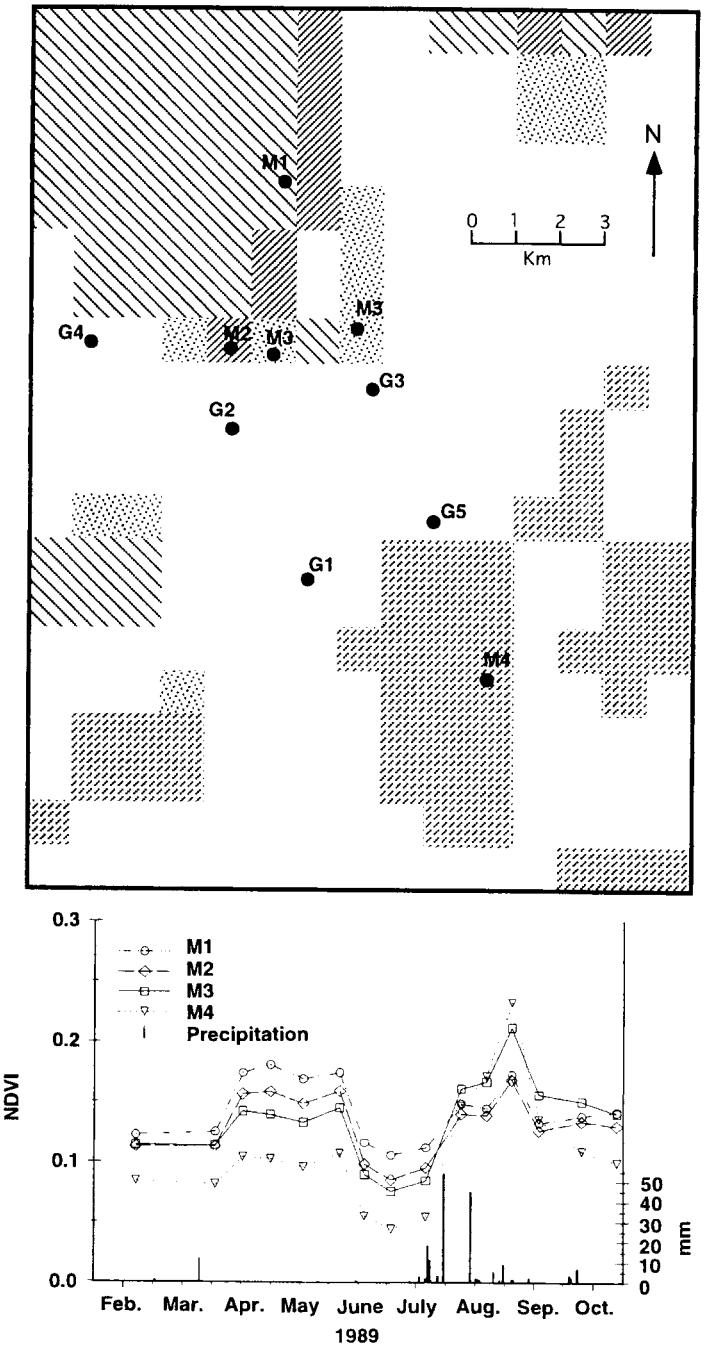

Fig. 7. Location of the mixed grass/shrub (M) vegetation communities best represented on the Jornada Experimental Range field calibration area and sites used for vegetation analysis. The range of normalized difference vegetation index (NDVI) values permits the designation of four vegetation subclasses within the mixed grass/shrub category. These are shown by distinctive shading patterns. Note that the field calibration sites, M1–M4, are located one in each of the four subclasses. Precipitation was recorded on the Rabbit rain gauge (R. P. Gibbens, unpublished data).

(Thurb) Rydb. (Mesa dropseed) (Gibbens 1991) and *H. mutica* will produce spring growth. While individual species may contribute to only a small portion of the canopy cover within a given community (Table 2), satellite observations are based on the total vegetative cover within the plant community (Table 3). Differences in the temporal dynamics of the plant communities are indicative of different mixes of plant species between communities.

ANALYSIS OF THE MIXED GRASS/SHRUB CLASSES

Sites within the Jornada field calibration area identified as mixed grass/shrub are shown on Fig. 7. The species mix and cover composition of representative sites are summarized in Tables 2 and 3. Precipitation graphs were derived from the daily rainfall records at the Rabbit rain gauge (location shown on Fig. 6) (R. P. Gibbens, unpublished data).

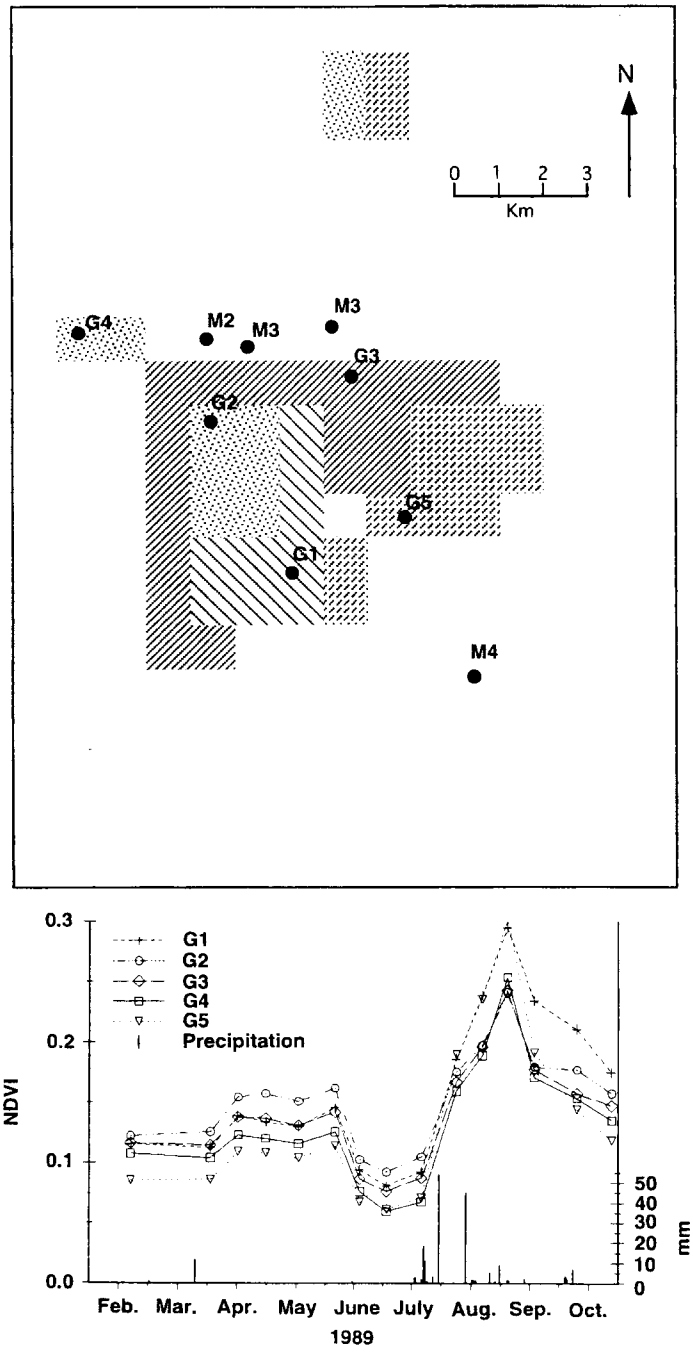

Fig. 8. Location of the grass (G)-dominated communities best represented on the Jornada Experimental Range field calibration area and sites used for vegetation analysis. The range of NDVI values present in the data permits the designation of four vegetation subclasses within the general grass category. These are shown by distinctive shading patterns, which should not be confused with the similarly shaded mixed grass/shrub subclasses shown in Fig. 7. Precipitation was recorded at the Rabbit rain gauge (R. P. Gibbens, unpublished data).

Class M1 in the mixed grass/shrub category (Fig. 7 and Table 3) was *P. glandulosa* coppice dunes. Vegetation information from the JER indicated that of the 36% cover, over 31% was *P. glandulosa* with 3% other shrubs and less than 2% cover of perennial C_4 grasses (Tables 2 and 3). The seasonal NDVI pattern of this class exhibited a strong peak in late April to early June, which is the period of leaf set and active growth of *P. glandulosa* in southern New Mexico (W. G. Whitford, unpublished data). The typical early summer depression of photosynthesis and subsequent increase in photosynthetic activity in late summer coincident with summer rains in this class failed to reach the level of the spring peak. The failure to reach the level of the spring peak was due to the extremely low cover of C_4 grasses that could produce a summer green peak and the small summer peak of mesquite leaf production response to monsoonal moisture (Nilsen *et al.* 1987). This late-season pattern was due to extremely low grass cover and represents primarily

Journal of Applied Ecology, **34**, 418–432

Table 2. Statistical summary of vegetation parameters at each field calibration site; data include the mean and standard deviation of percentage bare soil and plant cover by species (grouped according to photosynthetic mechanism: C_3, C_4 and crassulacean acid metabolism (CAM)) for each test site on the Jornada Experimental Range field calibration area

	% Bare soil		C_3*										C_4*												CAM*	
			Prgl		Flce		Atca		Lypa		Gusa		Scbr		Boer		Spfl		Arlo		Erpu		Mupo		Himu		Yuel	
Field site	$\bar{X}$	s	$\bar{X}$	s	$\bar{X}$	s	$\bar{X}$	s	$\bar{X}$	s	$\bar{X}$	s	$\bar{X}$	s	$\bar{X}$	s	$\bar{X}$	s	$\bar{X}$	s	$\bar{X}$	s	$\bar{X}$	s	$\bar{X}$	s	$\bar{X}$	s
G1	73·36		—		—		—		—		0·62		13·97		—		--		1·94		0·73		—		8·67		0·53	
		3·58		—		—		—		—		0·89		3·58		—		—		1·96		0·94		—		9·95		1·07
G2	56·87		0·71		—		—				1·78		—		34·19		0.58		3·95†		0·23		—		—		0·86	
		5·77		0·64		—		—		--		1·67		—		4·39		0·13		0·99		0·31		—		—		1·49
G3	73·70		12·70		—		1·29		—		3·38		—		0·03		5·80		0·20		2·88		0·04		—		—	
		3·05		4·30		—		2·48				2·17		—		0·06		3·55		0·16		2·62		0·05		—		—
G4	46·92		1·46		—		—		—		1·43		—		43·17		2·70		2·32†		0·30		—		—		1·26	
		8·01		1·55		—		—		—		0·76		—		9·32		1·31		2·38		0·06		—		—		1·08
G5	68·70		1·91				—		—		4·31		0·04		13·14		5·37		5·57		—		0·20		0·10		0·62	
		6·50		2·20		--		—		—		2·71		0·08		4·47		2·38		2·34		—		0·40		0·19		1·17
M1	63·37		31·49		—		1·40		—		1·90				—		0·72		0·06		0·46		0·35		—		0·25	
		8·06		8·36		—		1·66		—		0·75		—		—		0·91		0·09		0·63		0·80		—		0·80
M2	66·94		19·19		—		—				9·21		—		0·32		2·36		0·23†		0·71		0·08		—		0·15	
		6·69		5·04		—		—		—		5·30		—		0·64		1·32		0·24		0·60		0·16		—		0·17
M3	77·03		13·14		—		—		—		1·37		—		2·16		4·59		0·13		0·05		—		—		0·93	
		10·55		2·95		—		—		—		0·42		—		2·31		3·62		0·18		0·06		—		—		1·31
M4	37·97		—		17·59		—		12·94		0·09		11·60		—		0·02		—		—		15·88		3·18		0·06	
		11·11		—		3·10		—		5·26		0·14		4·89		—		0·07		—		--		7·27		7·45		0·17

*Other species not listed make up less than 1% total.

†Arlo and Arte combined.

$\bar{X}$ = mean; s = standard deviation. Prgl, *Prosopis glandulosa*; Flce, *Flourensia cernua*; Atca, *Atriplex canescens*; Lypa, *Lycium pallidum*; Gusa, *Guitierrezia sarothrae*; Scbr, *Scleropogon brevifolius*; Boer, *Bouteloua eriopoda*; Spfl, *Sporobolus flexuosus*; Arlo, *Aristida longiseta*; Arte, *Aristida ternipes*; Erpu, *Erioneruron pulchellum*; Mupo, *Muhlenbergia porteri*; Himu, *Hilaria mutica*; Yeul, *Yucca elata*.

Table 3. Summary of percentage plant cover by photosynthetic pathway for each vegetation type located on the Jornada Experimental Range field calibration area

Field site	Cover (%)	C_3 cover (%)	C_4 cover (%)	CAM cover (%)
G1	26·64	0·62	25·31	0·53
G2	43·13	2·49	38·95	0·86
G3	26·30	17·37	8·95	0·00
G4	53·08	2·89	48·49	1·26
G5	31·30	6·22	24·42	0·62
M1	36·63	34·79	1·59	0·25
M2	33·06	28·40	3·70	0·15
M3	22·97	14·51	6·93	0·93
M4	62·03	30·62	30·68	0.06

the response of mesquite to monsoonal moisture and the dropping temperatures of late summer and early autumn.

Classes M2 and M3 represent ecotonal areas between grasslands and the *P. glandulosa* dunes (Fig. 7 and Table 3). Of the two classes, M3 had significantly less cover of *P. glandulosa* and *G. sarothrae* and nearly double the grass cover recorded in class M2 (Table 3). Higher grass cover in class M3 largely accounted for the higher NDVI late summer peak and lower mesquite cover for the lower spring NDVI peak.

Class M4 represents an area with the shrubs *F. cernua* and *Lycium pallidum* Miers. (Solan.) (wolfberry) and a high percentage cover of perennial grasses (Tables 2 and 3). Because 1989 experienced a dry winter–spring, this class produced a seasonal NDVI curve characteristic of a grassland. During the drought, photosynthetic activity of *F. cernua* was minimal and leaves were small. When summer rains began in July, *F. cernua* and *L. pallidum* produced a new set of leaves. The high summer peak in this class was the addition of the shrub leaf area to the green tissue produced by the grasses listed in Table 2.

ANALYSIS OF THE GRASS-DOMINATED CLASSES

The grass-dominated communities showing the largest NDVI peaks in the summer rainy season (G1 and G5) were areas with essentially zero C_3 shrub cover (Fig. 8, Tables 2 and 3). The site within the field calibration area on the JER that was classified as class G5 had been treated with 2,4,5-T herbicide in 1988, resulting in die-back of nearly 100% of *P. glandulosa*. The 2% shrub cover of mesquite recorded in the 1994 vegetation sampling was regrowth from the root crowns of the *P. glandulosa* shrubs that were defoliated in 1988. The remaining C_3 shrub cover was *G. sarothrae*, which exhibits very little if any leaf production in dry winter–spring years. Class G1 was dominated by *S. brevifolia* and *H. mutica* with virtually no C_3 shrub cover.

Class G3 was ecotonal in its landscape position and composition. Its plant composition and NDVI graph characteristics were similar to class M3. The main differences were that G3 had slightly less bare soil, more C_4 grasses, and a higher monsoonal NDVI response (Figs 7 and 8, Tables 2 and 3). The other two grassland classes (G2 and G4) varied in C_3 shrub cover and generally had high cover of *B. eriopoda* (Torr.) Torr. (black grama). Despite high cover values of *B. eriopoda*, the NDVI peak in the rainy season was not as high as the burrograss and mixed grass classes. We think this is a function of the growth habit of *B. eriopoda*: most of the area of the grass clump is dead material from previous years' growth that gives the clump a dark, almost black appearance. The standing dead material in such clumps can mask the green of the current year's growth, resulting in a lower NDVI signal than expected on the basis of basal cover of the grass.

As in the case of the mixed grass/shrub category, we found that the classes of the grassland category derived from the unsupervised multitemporal image classification of the corresponding subset of the satellite imagery, were very similar to distinct areas of species cover on the JER. Thus our analysis shows that categories of desert biomass derived from multitemporal satellite imagery bear a close correspondence to the major species of plants identified from ground observations.

EXTRAPOLATION TO FIELD TEST AREA

Vegetation classes that were measured in our JER field calibration area were extrapolated to our larger field extrapolation area located to the west of the JER (Fig. 1). This location was selected because of prior knowledge of the area, accessibility and co-operative JER research in progress. Within the field extrapolation area we used distances from road intersections and/or topographic features to locate map units and walked varying distances to obtain a qualitative assessment of the vegetation in each pixel mapped area.

Classes M2, M3 and G4 did not occur in readily accessible portions of the field extrapolation area and were not analysed. In comparing classes M1 and G1 between the JER and the extrapolation area we found that they were very similar in cover, composition and structure. M4 was the vegetation class on the Jornada that comprised the largest portion of the extrapolation area. The grass composition of class M4 was similar, with *F. cernua* and *L. pallidum* in varying densities. Class G2 was similar with the exception that the field extrapolation area had significant amounts of *H. mutica*. Consistent with the ecotonal nature of class G3 on the JER, the same class in the field extrapolation area represented a mixture of different *P. glandulosa* densities with less than 20% grass understorey. Class G5 was similar in composition but the field extrapolation area was slightly higher in per-

centage cover than the corresponding area on the JER. Overall, the vegetation classes in the field extrapolation area (Fig. 1) were very similar in plant cover and composition to corresponding classes on the JER field calibration area and we therefore draw the same conclusion: that the classes derived from unsupervised temporal classification of the satellite data correspond to distinct cover classifications in the field extrapolation area just as they did on the JER field calibration area.

Discussion

Successful mapping of arid environments will ultimately depend on the availability of appropriate technology and suitable data. We believe our methods have demonstrated that the classification of time-resolved satellite images, accompanied by field observations, has utility as a mapping tool. Our present efforts are directed to the improvement of the accuracy of vegetation classification using a refined atmospheric attenuation correction and, secondly, a technique for processing soil background variability, both on a per-pixel basis. Success in these areas will improve our ability to calibrate biophysical parameters in these areas of arid ecosystems. Plant growth in the Chihuahuan Desert is highly variable and dependent on moisture availability (Peters & Eve 1995). A complete evaluation of desertification processes would require the incorporation of additional years of data and expanded field verification. In the meantime, we have shown that the use of seasonal patterns of satellite-derived vegetation indices to classify and analyse growth dynamics of desert vegetation has provided a reliable map of several northern Chihuahuan Desert grassland and shrubland communities.

Acknowledgements

This study was funded in part by the US Environmental Protection Agency, Environmental Monitoring Systems Laboratory, Las Vegas, Nevada. The research described herein has not been subjected to the agency's peer and administrative review. Therefore the conclusions and opinions are solely those of the authors and should not be construed to reflect the views of the agency.

References

Bastin, G.N., Pickup, G. & Pearce, G. (1995) Utility of AVHRR data for land degradation assessment: a case study. *International Journal of Remote Sensing*, **16**, 651–672.

Buell, M.F. & Cantlon, J.E. (1950) A study of two communities of the New Jersey Pine Barrens and a comparison of methods. *Ecology*, **31**, 567–586.

Buffington, L.C. & Herbal, C.H. (1965) Vegetational changes on a semidesert grassland range from 1858 to 1963. *Ecological Monographs*, **35**, 139–164.

Canfield, R. (1941) Application of the line interception method in sampling range vegetation. *Journal of Forestry*, **39**, 388–394.

Di, L. & Rundquist, D.C. (1994) An one-step algorithm for correction and calibration of AVHRR level 1b data. *Photogrammetric Engineering* and *Remote Sensing*, **60**, 165–171.

Eidenshink, J.C. & Hass, R.H. (1992) Analyzing vegetation dynamics of land systems with satellite data. *Geocarto International*, **1**, 53–61.

Elvidge, C.D. & Lyon, R.J.P. (1985) Influence of rock-soil spectral variation on assessment of green biomass. *Remote Sensing of Environment*, **17**, 265–279.

Fisher, F.M., Zak, J.C., Cunningham, G.L. & Whitford, W.G. (1988) Water and nitrogen effects on growth and allocation patterns of creosotebush in the northern Chihuahuan Desert. *Journal of Range Management*, **41**, 387–391.

Frank, T.D. (1985) Differentiating semiarid environments using landsat reflectance indexes. *Professional Geographer*, **37**, 36–46.

Gibbens, R.P. (1991) Some effects of precipitation patterns on mesa dropseed phenology. *Journal of Range Management*, **44**, 86–90.

Goward, S.N., Tucker, C.J. & Dye, D.G. (1985) North American vegetation patterns observed with the NOAA-7 advanced very high resolution radiometer. *Vegetatio*, **64**, 3–14.

Holben, B.N. (1986) Characteristics of maximum-value composite images from temporal AVHRR data. *International Journal of Remote Sensing*, **7**, 1417–1434.

Huete, A.R. & Jackson, R.D. (1987) Suitability of spectral indices for evaluating vegetation characteristics on arid rangelands. *Remote Sensing of Environment*, **23**, 213–232.

Jensen, J.R. (1995) *Introductory Digital Image Processing*. Prentice Hall, New Jersey.

Justice, C.O., Townshend, J.R.G., Holben, B.N. & Tucker, C.J. (1985) Analysis of the phenology of global vegetation using meteorological satellite data. *International Journal of Remote Sensing*, **6**, 1271–1318.

Lambin, E.F. & Strahler, A.N. (1994) Change-vector analysis in multitemporal space: a tool to detect and categorize land-cover change processes using high temporal-resolution satellite data. *Remote Sensing of Environment*, **48**, 231–244.

Lillesand, T.M. & Kiefer, R.W. (1994) *Remote Sensing and Image Interpretation*. John Wiley, New York.

Millington, A.C. & Pye, K. (1994) Biogeographical and geomorphological perspectives in environmental change in drylands. *Environmental Change in Drylands* (eds A. C. Millington & K. Pye), pp. 427–441. John Wiley & Sons Ltd, Chichester.

Millington, A.C., Critchley, R.W., Douglas, T.D. & Ryan, P., Eds. (1994a) *Estimating Woody Biomass in sub-Saharan Africa*. World Bank, Washington, DC.

Millington, A.C., Wellens, J., Settle, J.J. & Saull, R.J. (1994b) Explaining and monitoring land cover dynamics in drylands using multi-temporal analysis of NOAA AVHRR imagery. *Environmental Remote Sensing from Regional to Global Scales* (eds G. M. Foody & P. J. Curran), pp. 16–43. John Wiley & Sons Ltd, Chichester.

Nilsen, E.T., Sharifi, M.R., Virginia, R.A. & Randel, P.W. (1987) Phenology of warm desert phreatophytes: seasonal growth and herbivory in *Prosopis glandulosa* var. *torreyana* (honey mesquite). *Journal of Arid Environments*, **13**, 217–229.

NOAA (1989) *Climatatological Data New Mexico*, Vol. 93.

NOAA (1991) *NOAA Polar Orbiter Data User's Guide*. US

Department of Commerce, NOAA, NESDIS, NCDC, and the Satellite Data Services Division, Washington, DC.

Paulsen, H.A. & Ares, F.N. (1962) Grazing values and management of black grama and tobosa grasslands and associated shrub ranges of the southwest. *Technical Bulletin no. 1270*, US Department of Agriculture, Forest Service, Washington, DC.

Peters, A.J. & Eve, M.D. (1995) Satellite monitoring of desert plant community response to moisture availability. *Environmental Monitoring and Assessment*, **37**, 273–287.

Peters, A.J., Reed, B.C., Eve, M.D. & Havstad, K.M. (1993) Satellite assessment of drought impact on native plant communities of southeastern New Mexico, USA. *Journal of Arid Environments*, **24**, 305–319.

Pickup, G. (1994) Modelling patterns of defoliation by grazing animals in rangelands. *Journal of Applied Ecology*, **31**, 231–246.

Pickup, G. (1995) A simple model for predicting herbage production from rainfall in rangelands and its calibration using remotely sensed data. *Journal of Arid Environments*, **30**, 227–245.

Pickup, G. & Chewings, V.H. (1994) A grazing approach to land degradation assessment in arid areas from remotely sensed data. *International Journal of Remote Sensing*, **15**, 597–617.

Stephens, G. & Whitford, W.G. (1993) Responses of *Bouteloua eripoda* to irrigation and nitrogen fertilization in a Chihuahuan desert grassland. *Journal of Arid Environments*, **24**, 415–421.

Tucker, C.J. (1979) Red and photographic infrared linear combinations for monitoring vegetation. *Remote Sensing of Environment*, **8**, 127–150.

Tucker, C.J. & Choudhury, B.J. (1987) Satellite remote sensing of drought conditions. *Remote Sensing of Environment*, **23**, 243–251.

Tucker, C.J., Dregne, H.E. & Newcomb, W.W. (1991) Expansion and contraction of the Sahara desert from 1980 to 1990. *Science*, **253**, 299–301.

Tucker, C.J., Townshend, J.R.G. & Goff, T.E. (1985) African land-cover classification using satellite data. *Science*, **227**, 369–375.

Turner, M.G. (1989) Landscape ecology: the effect of pattern on process. *Annual Review of Ecological Systematics*, **20**, 171–197.

US Environmental Protection Agency (1994) *Landscape Monitoring and Assessment Research Plan*. US EPA 620/R-94/009, Washington, DC.

Received 4 July 1995; revision received 29 June 1996